Optical Stokes Flow: An Imaging-Based Control Approach

Paul Ruhnau, Christoph Schnörr

Department of Mathematics & Computer Science, University of Mannheim, 68131 Manheim, Germany,
{ruhnau,schnoerr}@uni-mannheim.de

Abstract We present an approach to particle image velocimetry based on optical flow estimation subject to physical constraints. Admissible flow fields are restricted to vector fields satisfying the Stokes equation.The latter equation includes control variables that allow to control the optical flow so as to fit to the apparent velocities of particles in a given image sequence. We show that when the real unknown flow observed through image measurements conforms to the physical assumption underlying the Stokes equation, the control variables allow for a physical interpretation in terms of pressure distribution and forces acting on the fluid. Although this physical interpretation is lost if the assumptions do not hold, our approach still allows for reliably estimating more general and highly non-rigid flows from image sequences.

1. Introduction

1.1. Motivation and Overview

Recently, a novel class of variational approaches to image fluid analysis has been introduced in [**19**, **8**, **18**]. These methods are based on approaches originally developed in the field of computer vision [**6**, **12**, **20**] and suitable elaborated and modified for the purpose of PIV. The prototypical approach presented in [**19**] was most recently improved in [**3**] by taking into account higher-order regularization. For recent improvements concerning correlation-based PIV techniques, we refer to [**14**, **13**] and references therein.

The basic idea of variational optical flow approaches is not to estimate displacement vectors locally and individually, but to estimate vector fields as a whole by minimizing a suitable functional defined over the entire image section. Besides yielding dense flows with a high spatial resolution, a key advantage of these methods is that they allow for the robust estimation of coherent flows by including variational penalty terms that enforce spatial or temporal smoothness of the minimizing vector fields.

In this work, we study a novel optical flow-based approach to *Particle Image Velocimetry (PIV)* that incorporates physical prior knowledge in a more precise and explicit way: All admissible flows for estimation have to satisfy the Stokes equation. In order to estimate the specific flow of apparent velocities of particles in an image sequence, control variables are included and determined by minimizing a suitable objective function which relates the flow and the control variables to given image sequence data. We show that our approach not only estimates the flow from a given PIV image sequence, but pressure and forces acting on the real fluid as well, provided the real flow satifies the Stokes equation too.

1.2. Related Work

Our approach draws on the general literature on control of distributed parameter systems [**10**]. For specific approaches in connection with fluid dynamics, we refer to [**4**]. The application of flow

control techniques to image motion estimation, as presented in this paper, is novel, however.

Concerning the incorporation of physical constraints for flow estimation through image processing, several interesting approaches have been suggested in the past. Combining PIV and CFD by using cost functions were proposed in [**7**,**15**]. In contrast to our approach, they can be understood as *post*-processing methods: By correcting cross-correlation velocity estimates such that they satisfy the incompressible Navier-Stokes equations, outliers are reliably detected and rectified.

More recently, physics-based non-linear dynamic models [**17**] have been introduced to PIV.
The velocity is again obtained by minimizing a measure which consists of the residues of the Navier-Stokes equation, the continuity equation, and the difference between estimated and observed image data. The resulting non-linear optimization system is solved using methods from evolutionary programming [**11**]. This procedure is repeated until the difference between the observed and the estimated image is sufficiently small. This method allows a reliable estimation of velocity fields and pressure estimates. One may criticize, however, that little insight can be gained from the viewpoint of optimization.

The reader may ask: Why we do confine ourselves to Stokes flows, as opposed to flows governed by the full Navier-Stokes equation? In this connection, we wish to point out that we consider, for the first time to our knowledge, a quite difficult *inverse* problem – the joint estimation of a flow along and related physical quantities. This problem is intricate through the *interaction* of various components, although each of them behaves in a mathematically simple way. Therefore, to study the computational feasibility and robustness, we have chosen Stokes flows as a first step.

1.3. Organization

In section 2 we will present the constrained minimization problem that is solved - along with the control approach that is used for optimization. We will illustrate the finite element discretization and the applied numerics. Next, we will examine features of a coarse-to-fine implementation (sec. 3.2). Numerical experiments on ground-truth image pairs as well as on real-world image sequences will be presented in section 4. We conclude in section 5 by indicating extensions within the variational control framework.

2. Approach

2.1. Constrained Variational Optical Flow Estimation

Let $I(x,y,t)$ denote the grayvalue recorded at location $(x,y)^\top$ and time t in the image plane. A basic assumption underlying most approaches to motion estimation is that I is conserved, that is the change of $I(x,y,\cdot)$ at location $(x,y)^\top$ is due to a movement of $I(x,y,t)$ to the location $(x+u\Delta t, y+v\Delta t)^\top$ during a time interval Δt:

$$I(x+u\Delta t, y+v\Delta t, t+\Delta t) \approx I(x,y,t)\,. \tag{1}$$

Here, $\mathbf{u}=(u,v)^\top$ denotes the *optical flow*, that is the apparent instantaneous velocity of image structures. The frame rate Δt is assumed to be small, so that $\mathbf{u}\Delta t$ is close to the actual displacement. In the following, we put $\Delta t = 1$ without loss of generality.
In view of various influences like noise which affect the validity of (1), the common approach is to consider the squared error over the entire image domain Ω:

$$\int_\Omega [I(x+u(x,y), y+v(x,y), t+1) - I(x,y,t)]^2 \, dxdy \tag{2}$$

From the viewpoint of variational analysis and algorithm design, formulation (2) is not convenient, however, because the dependency on u and v is non-convex. A common way around this difficulty is (i) to further approximate the objective function so as to obtain a mathematically tractable problem, and (ii) to apply the resulting variational approach to a multi-scale representation of the image data I. Point (i) is addressed by a Taylor series linearization of (2) and dropping the argument (x, y, t) for convenience:

$$\int_\Omega [\nabla I \cdot \mathbf{u} + \partial_t I]^2 \, dxdy \tag{3}$$

The spatial and temporal derivatives of I can be estimated locally using FIR filters. Point (ii) above is briefly sketched in section 3.2. For a more detailed account, we refer to [**19**].
Problem (3) is not well-posed because any vector field with components $\nabla I \cdot \mathbf{u} = -\partial_t I, \forall x, y$, is a minimizer. The standard approach is to add a variational term enforcing smoothness of the flow [**6**]:

$$\int_\Omega \{(\nabla I \cdot \mathbf{u} + \partial_t I)^2 + \alpha(|\nabla u|^2 + |\nabla v|^2)\} dxdy \tag{4}$$

In this paper, we investigate an alternative method. Rather than penalizing the estimated flow with a smoothness term, we require as an additional constraint that (3) should be minimized subject to the time-independent divergence-free Stokes system describing the steady motion of viscous media:

$$\begin{cases} -\mu\Delta\mathbf{u} + \nabla p &= \mathbf{f} \quad \text{in } \Omega, \\ \nabla \cdot \mathbf{u} &= 0 \quad \text{in } \Omega, \\ \mathbf{u} &= \mathbf{g} \quad \text{on } \Gamma \end{cases} \tag{5}$$

Here, p denotes the pressure, μ the constant kinematic viscosity, $\mathbf{f}$ the body force acting on the fluid, and $\mathbf{g}$ the boundary values.
Our objective is to determine a body force **f** and boundary values **g** that yield a velocity field **u** which matches the apparent motion (measured by (3)) as good as possible. Note, however, that the minimization of (3) subject to (5) only enforces vanishing divergence of the flow **u**. The diffusion term in (5) has no impact because **f** and **g** can be chosen such that *every* divergence-free velocity field satifies the Stokes equation. Therefore, we additionally regularize **f** and **g**, rendering the whole system mathematicaly well-posed. As a result, we finally obtain the objective functional

$$J(\mathbf{u}, p, \mathbf{f}, \mathbf{g}) = \int_\Omega \frac{1}{2}[\nabla I \cdot \mathbf{u} + \partial_t I]^2 d\mathbf{x} + \int_{\Omega \setminus \Omega_0} \frac{\alpha}{2} |\mathbf{f}|^2 \, d\mathbf{x} + \int_\Gamma \frac{\gamma}{2} |\nabla_\Gamma \mathbf{g}|^2 \, d\Gamma \tag{6}$$

which is to be minimized subject to (5). Ω_0 in the second term in (6) denotes regions in the image where we expect large forces acting on the fluid (e.g. interfaces with solids). Therefore, we exclude body force penalization at these locations. $\nabla_\Gamma \mathbf{g}$ denotes the derivative of **g** tangential to the boundary.
In terms of control theory (e.g. [**4**]), the approach can be summarized as follows: We wish to find an optimal state $(\mathbf{u}, p)$ and optimal distributed controls $(\mathbf{f}, \mathbf{g})$ such that functional J (6) is minimized subject to $\mathbf{u}, p, \mathbf{f}$ and $\mathbf{g}$ satisfying the Stokes system (5).

2.2. Optimality Condition

To derive the optimality system for determining optimal solutions to (6), (5), we transform the constrained optimization problem into an unconstrained optimization with the Lagrangian function

$$L(\mathbf{u}, p, \mathbf{f}, \mathbf{g}, \mathbf{w}, r, \xi) = J(\mathbf{u}, p, \mathbf{f}, \mathbf{g}) - \int_\Omega \mathbf{w}^\top(-\mu\Delta\mathbf{u} + \nabla p - \mathbf{f}) + r(\nabla\cdot\mathbf{u})d\mathbf{x} - \int_\Gamma \xi^\top(\mathbf{u}-\mathbf{g})d\Gamma \quad (7)$$

and corresponding multipliers $\mathbf{w}, r, \xi$. The first-order necessary conditions then yield the optimality system which determines optimal states and controls:

$$\begin{cases} -\mu\Delta\mathbf{u} + \nabla p &= \mathbf{f} \quad \text{in } \Omega \\ \nabla\cdot\mathbf{u} &= 0 \quad \text{in } \Omega \\ \mathbf{u} &= \mathbf{g} \quad \text{on } \Gamma \end{cases} \quad (8a)$$

$$\begin{cases} \mu\Delta\mathbf{w} + \nabla r &= -(\nabla I^\top\mathbf{u} + \partial_t I)\nabla I \quad \text{in } \Omega \\ \nabla\cdot\mathbf{w} &= 0 \quad \text{in } \Omega \\ \mathbf{w} &= 0 \quad \text{on } \Gamma \end{cases} \quad (8b)$$

$$\begin{cases} \mathbf{w} + \alpha\mathbf{f} &= 0 \quad \text{in } \Omega\backslash\Omega_0 \\ \mathbf{w} &= 0 \quad \text{in } \Omega_0 \\ r\mathbf{n} - \mu\partial\mathbf{w}/\partial\mathbf{n} - \gamma\Delta_\Gamma\mathbf{g} &= \mathbf{g} \quad \text{on } \Gamma \end{cases} \quad (8c)$$

where $\Delta_\Gamma\mathbf{g}$ is the 1D laplacian of $\mathbf{g}$ tangential to the boundary.

The *state equation* (8a) results from taking the Gâteaux derivative of (7) in the direction of the Lagrange multipliers, reproducing the Stokes equation (5). Equation (8b) is the *adjoint equation*. It specifies the first-order necessary conditions with respect to the state variables $\mathbf{u}$ and p. Note that this equation has the same structure as (8a) with just the variables replaced by the adjoint velocity $\mathbf{w}$ and the adjoint pressure r. Consequently, we can use the same numerical algorithm to solve (8a) and (8b). The third system of equations (8c) states the *optimality condition* which is the necessary condition that the gradient of the objective functional with respect to the controls vanishes at the optimum.

We state next the optimization problem for solving (8). Discretization and numerical solution of subproblems (8a) and (8b) are detailed in section 3.1.

2.3. Optimization Algorithm

Due to the large number of unknowns in the optimality system (8), we decouple the state system (8a) and the adjoint system (8b), and apply the gradient method for computing the solution of the optimal control problem.

We start with a velocity field $\mathbf{u} = 0$ (or with any other initial value) and solve the adjoint equation. Computing the gradient of the functional with respect to $\mathbf{g}$ and $\mathbf{f}$, respectively, yields

$$\partial_\mathbf{f} J = \mathbf{w} + \alpha\mathbf{f} \quad (9a)$$

$$\partial_\mathbf{g} J = r\mathbf{n} - \mu\frac{\partial\mathbf{w}}{\partial\mathbf{n}} - \gamma\Delta_\Gamma\mathbf{g} - \frac{\mathbf{n}}{|\Gamma|}\int_\Gamma(-\mu\frac{\partial\mathbf{w}}{\partial\mathbf{n}} + r\mathbf{n} - \gamma\Delta_\Gamma\mathbf{g})\cdot\mathbf{n}d\Gamma = 0 \quad (9b)$$

Note that r is determined by the adjoint equation (8b) only up to a constant. (9b) chooses this constant such that the update of $\mathbf{g}$ satisfies the compatibility condition $\int_\Gamma \mathbf{g}\cdot\mathbf{n}d\Gamma = 0$ (sum of

inflow = sum of outflow). Having updated the controls, we solve the state equation and proceed to the next iteration. After convergence of the algorithm, the iterates satisfy (8c), too.
Experiments have shown that using two individual and adaptive step sizes for $\mathbf{f}$ and $\mathbf{g}$, respectively, is computationally both more reliable and efficient.

3. Discretization and Implementation

3.1. Solving the Subproblems

In every iteration of the algorithm descried in sec. 2.3., we have to solve two saddle point problems corresponding to the state equation (8a) and to the adjoint equation (8b), respectively. In this section, we explain how these problems are discretized and numerically solved.
The unique vector field $\mathbf{u}(x, y)$ solving (8a) is determined by the variational system

$$\begin{aligned} a(\mathbf{u},\tilde{\mathbf{u}}) + b(p,\tilde{\mathbf{u}}) &= (\mathbf{f},\tilde{\mathbf{u}}), \quad \forall \tilde{\mathbf{u}} \\ b(\tilde{\mathbf{p}},\mathbf{u}) &= 0, \quad \forall \tilde{\mathbf{p}} \end{aligned} \tag{10}$$

and a similar variational system determines the unique solution $\mathbf{w}$ to (8b). Accordingly, we define for the Stokes problem and for the adjoint problem, respectively, bilinear forms and linear forms:

$$a_{St}(\mathbf{u},\tilde{\mathbf{u}}) := \int_\Omega \mu \nabla \mathbf{u} \cdot \nabla \tilde{\mathbf{u}} d\mathbf{x} \qquad a_{Adj}(\mathbf{w},\tilde{\mathbf{w}}) := \int_\Omega -\mu \nabla \mathbf{w} \cdot \nabla \tilde{\mathbf{w}} d\mathbf{x} \tag{11}$$

$$b_{St}(p,\tilde{\mathbf{u}}) := -\int_\Omega p \nabla \cdot \tilde{\mathbf{u}} d\mathbf{x} \qquad b_{Adj}(r,\tilde{\mathbf{w}}) := -\int_\Omega r \nabla \cdot \tilde{\mathbf{w}} d\mathbf{x} \tag{12}$$

and the right hand sides:

$$(\mathbf{f}_{St},\tilde{\mathbf{u}}) := \int_\Omega \mathbf{f} \cdot \tilde{\mathbf{u}} d\mathbf{x} \qquad (\mathbf{f}_{Adj},\tilde{\mathbf{w}}) := \int_\Omega -(\nabla I^\top \mathbf{u} + \partial_t I) \nabla I \cdot \tilde{\mathbf{w}} d\mathbf{x} \tag{13}$$

We choose a regular tesselation of the image domain Ω and discretize (10) using finite elements. It is well-known from computational fluid dynamics that standard first-order finite element discretizations may result in non-physical pressure oscillations or even in so-called locking effects, where the zero velocity field is the only one satisfying the incompressibility condition.

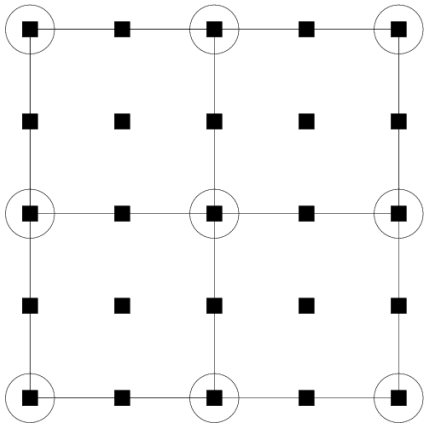

Fig. 1. Sketch of 2D Taylor-Hood elements: biquadratic velocity elements (squares) and bilinear pressure elements (circles).

Therefore, when solving the Stokes Problem, mixed finite elements are traditionally used. An admissible choice is the so-called Taylor-Hood element based on a square reference element with nine nodes (Figure 1). Each component of velocity fields is defined in terms of piecewise quadratic basis functions ψ located at each node, whereas pressure fields are represented by linear basis functions ϕ attached to each corner node. It can be shown that Taylor-Hood elements fulfill the so-called Babuska-Brezzi condition [**2**], that is the discretized problem is well-posed.

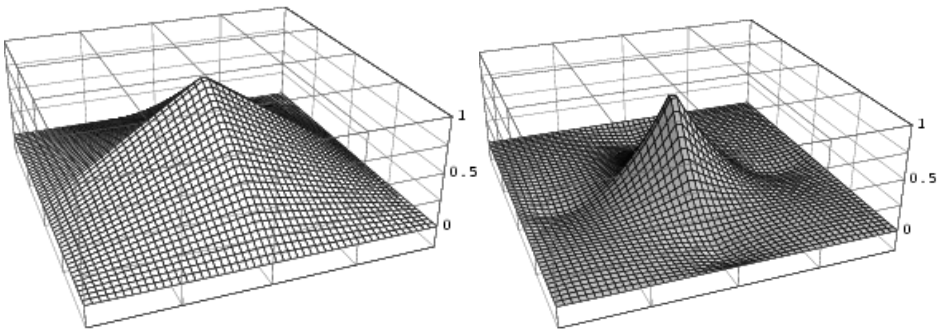

Fig. 2. Left: Basis function ϕ of a bilinear finite element. Right: Basis function ψ of a biquadratic finite element.

Applying a Taylor-Hood finite element discretization, we obtain the discretized Stokes system

$$\begin{aligned} A\mathbf{u} + B^{\top} p &= \mathbf{f} \\ B\mathbf{u} &= 0 \end{aligned} \tag{14}$$

and a similar system for the adjoint equation.
In order to numerically solve this saddle point problem, we employ the Uzawa algorithm (cf., e.g. [**1**]). Since the matrix A is positive definite, we solve the first equation of the system (14) for the unknown $\mathbf{u}$:

$$\mathbf{u} = A^{-1}(\mathbf{f} - B^{\top} p) \tag{15}$$

and insert the result in the second equation

$$BA^{-1}(\mathbf{f} - B^{\top} p) = 0 \tag{16}$$

This gives a problem which only incorporates the pressure

$$(BA^{-1}B^{\top})\, p = BA^{-1}\mathbf{f} \tag{17}$$

The matrix $(BA^{-1}B^{\top})$ is symmetric and positive definite. Therefore, we apply the conjugate gradient algorithm to (17). This requires a single matrix inversion in every iteration step. For computational efficiency, this is accomplished using a multigrid iteration (cf. [**5**]). Note that A is just the system matrix of the Poisson equation. For 2D problems, A can be split into two systems (one for every dimension), that can be solved in parallel.

3.2. Coarse-to-fine Approach

Due to the Taylor series linearization inherent in the optical flow constraint, only slow motion can be accurately computed by minimizing (3) (approx. up to 1 pixel per frame). This is why we apply our approach to a multi-scale representation of the image data I: We first compute a coarse motion field by using only low spatial frequency components and undo the motion, thus roughly stabilizing the position of the image over time. Then the higher frequency subbands are used to estimate the optical flow on the warped sequence. Combining this optical flow correction with the previously computed optical flow yields a refined overall optical flow estimate. This process is repeated at finer spatial scales until the original image resolution is reached.

Let $\mathbf{u}$ denote the overall velocity that results from our computations, $\mathbf{u}_{\mathbf{old}}$ the current estimate of this overall velocity, and $\partial_t I_w$ the temporal derivative computed as difference between the second image - warped with $\mathbf{u}_{\mathbf{old}}$ - and the first image. Then (3) can be reformulated as

$$J(\mathbf{u}) = \int_\Omega \frac{1}{2}(\nabla I^\top(\mathbf{u} - \mathbf{u}_{\mathbf{old}}) + \partial_t I_w)^2 d\mathbf{x} \tag{18}$$

This reformulation does not affect the state system and the optimality condition. The adjoint system, on the other hand, is transformed into

$$\begin{cases} \mu\Delta\mathbf{w} + \nabla r &= -(\nabla I^\top(\mathbf{u} - \mathbf{u}_{\mathbf{old}}) + \partial_t I_w)\nabla I & \text{in } \Omega \\ \nabla \cdot \mathbf{w} &= 0 & \text{in } \Omega \\ \mathbf{w} &= 0 & \text{on } \Gamma \end{cases} \tag{19}$$

We could now start at every resolution level with an initial zero velocity field. This is a poor initialization, however: We know that $\mathbf{u}_{old}$ is a good approximation of the true velocity field: Therefore, we solve (8a) for (**u**, p) before the first iteration of every resolution level, using interpolated versions of **f** and **g** from the preceding level. We obtain an initial velocity **u** that both satisfies (8a) and is a good approximation of the true velocity field.

4. Experimental Evaluation

In order to prove the validity of the concept of our approach and to identify possible drawbacks, we first test our approach on synthetic image pairs with underlying analytically computed velocity fields. Besides the question of the accuracy of our method, we want to go further into the question of how meaningful the asserted estimates for pressure p and body force $\mathbf{f}$ prove to be.

It should be noted that, because we use the Stokes equation as a physical model, it only makes sense to analyze velocity fields with very low Reynolds numbers. We will show later (section 4.2.) that one can also achieve good velocity estimates for highly non-rigid flows. In these cases, however, we cannot expect the body-force and the pressure distribution to contain physically relevant information.

4.1. Poiseuille Flow

We consider an incompressible Newtonian fluid with constant density and viscosity flows between two parallel plates (at $y = 0$ and $y = h$) with infinite width. The x-axis points in the direction of the flow. The velocity distribution for such a system is given by (e.g. [**9**])

$$u(y) = -\frac{1}{2\mu}\frac{\partial p}{\partial x}\left(\frac{h^2}{4} - \left(y - \frac{h}{2}\right)^2\right). \tag{11}$$

This means that we can expect a parabolic velocity profile, with the largest velocity in the middle between the two plates.

For our synthetic experiment, we chose $\mu = 1$, $h = 257\ px.$, and $\frac{\partial p}{\partial x} = -1 \cdot 10^{-3}$. This choice yields a maximum velocity of 8.256 px./frame. Figure 3 shows the synthetic image and the target velocity field with which the image was warped in order to get a synthetic image pair. We used the same techniques as described in [**16**] (10.000 particles, 3 px. average particle diameter, 1 px. standard deviation). As the Poiseuille flow is truly 2D, the third component is zero everywhere. Please note that while in numerical hydrodynamics one is accustomed to small mesh sizes ($s << 1$) and small volumes ($VOL \approx 1$), we measure in terms of pixels here. This is why the parameter choice may appear uncommon.

In a first experiment, we set $\alpha = 100$ and $\gamma = 200$, and we penalized the body force everywhere (i.e. $\Omega_0 = \varnothing$). Figure 4 shows the reconstructed velocity component u. The estimated velocity is almost exact (cf. also Fig. 7), its RMS error is $\approx 0.0734\,px$. However, Fig. 7 also shows that there are problems at the boundaries of the plates. They are caused by the forces acting on the fluid. In fact, the locations where forces act on the fluid are just the boundaries of the plates: The pressure-induced force acts orthogonal to the interfaces and is

$$f_x = -p\mathbf{n} \tag{12}$$

The frictional force at the interfaces acts in opposite flow direction and is

$$f_y = \frac{h}{2}\frac{\partial p}{\partial x} \tag{13}$$

Figure 5 (left) shows that the algorithm has in fact detected a force at the interfaces that acts in opposite flow direction. However, the method also detects a (smaller) force in the middle of the pipe that acts in flow direction. The reason for this error is quite obvious: In (6), we added constraints on the body force that penalize the L_2 norm of $\mathbf{f}$. The correct body force, however, has an extremely high L_2 norm at the interfaces. In order to yet compute a reliable body force – and thus also pressure estimates, as the pressure depends on velocity *and* body force – we have to tell the algorithm at what locations forces are likely to act on the fluid. Then we can exclude the body force penalization at these locations.

Accordingly, in a second experiment, we switched off body force penalization at the interfaces of the two parallel plates (at $y = 0$ and $y = h$). The results can be seen in figure 5 (right): The reconstructed body force is reasonable. Fig. 6 compares the estimated body force components and the analytically computed forces: Both the pressure-induced and the frictional forces are recovered accurately.

Figure 7 shows that also the RMS error has decreased considerably (RMS $\approx 0.0212\,px$). Note that there are still errors at the ends of the interfaces which can also be perceived in the forces of Fig. 6. The reason for these errors is regularization of the boundary values g (cf. (6)). The smoothness of the boundary values enforced by (6) deviates from reality at these locations.

Figure 4 shows the reconstructed pressure field on the right. Taking a closer look at the pressure derivative in flow direction (cf. Fig. 8), we see that the pressure derivative inside the tube is approx. $4 \cdot 10^{-3}$, which is the correct reconstruction. We point out that due to the mixed finite element discretization, the resolution of the pressure field is smaller than the resolution of the reconstructed velocity. Therefore, the pressure derivative has to be scaled with the factor 4.

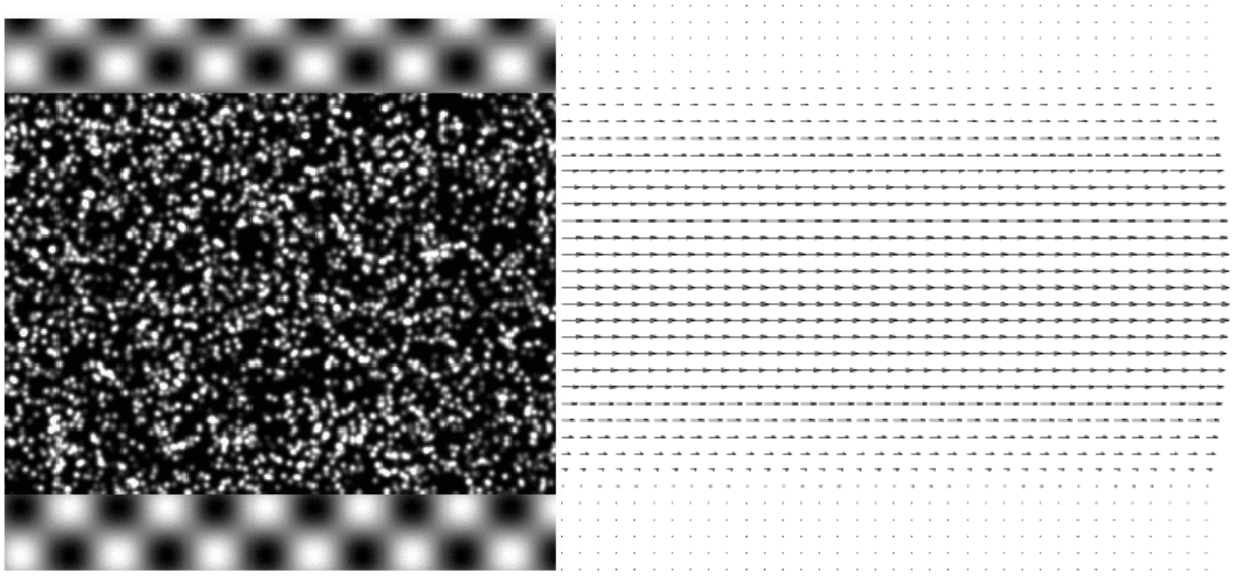

Fig. 3. Left: Synthetic PIV image. Right: Poiseuille velocity field.

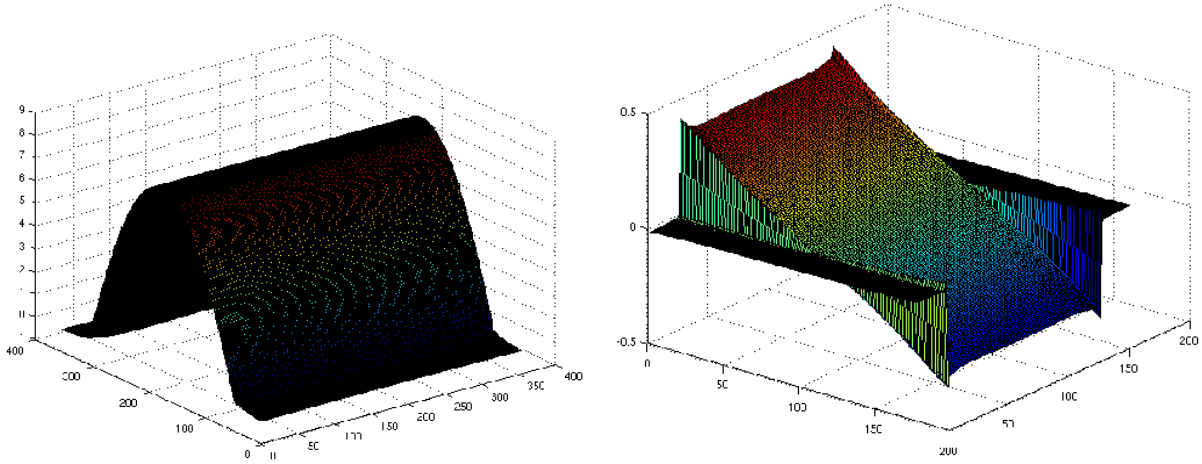

Fig. 4. Left: Reconstructed velocity field. Right: Reconstructed pressure field (no penalization of f at the interfaces).

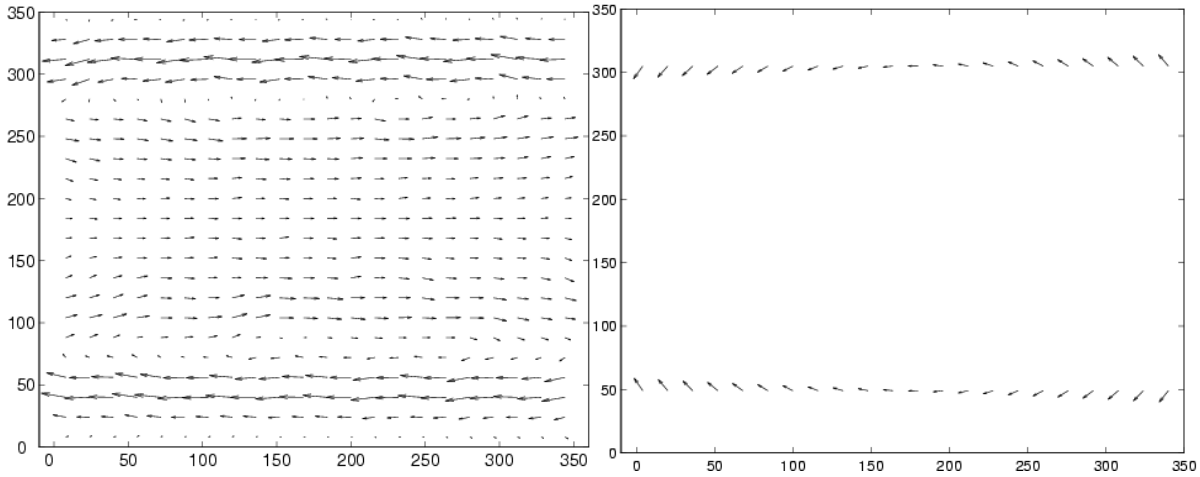

Fig. 5. Reconstructed body force. Note that the arrows are scaled in order to be visible. Left: f is penalized everywhere (scaling factor: 2000). Right: no penalization of f at the interfaces (scaling factor: 50).

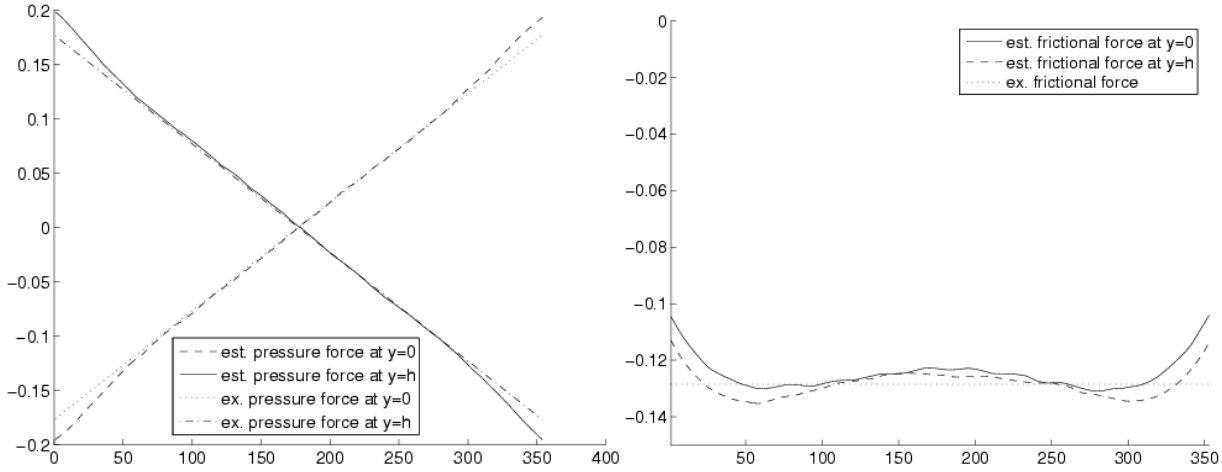

Fig. 6. Left: Pressure-induced force at $y=0$ and $y=h$ (estimated vs. exact). Right: Frictional force at $y=0$ and $y=h$ (estimated vs. exact).

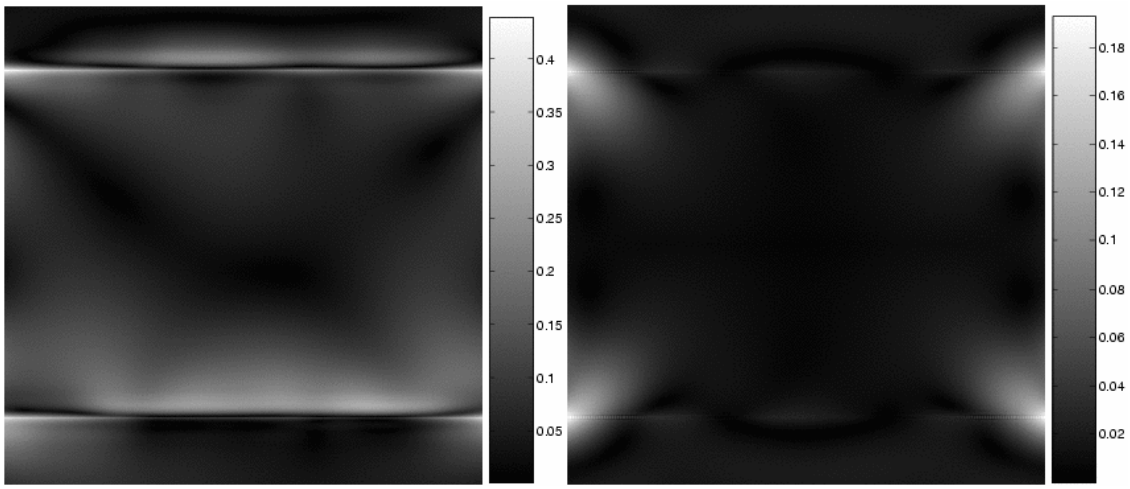

Fig. 7. Left: RMS error (f is penalized everywhere), mean = 0.0734 px. Right: RMS error (no penalization of f on the interfaces), mean = 0.0212 px.

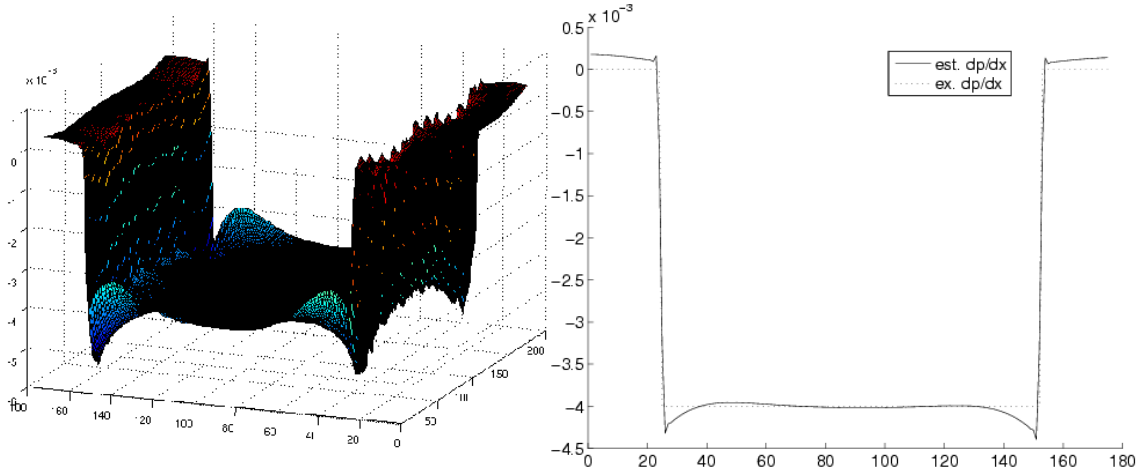

Fig. 8. Left: Derivative of the pressure field in flow direction. Right: Profile of the averaged pressure derivative.

4.2. Highly Non-Rigid Flow

Figure 9 shows the first image of a highly non-rigidly deformed image pair. We know that the underlying motion field is incompressible and has only an very small out-of-plane component. That is, we can assume incompressibility also in 2D. Note, however, that the velocity field is certainly not governed by the Stokes equation, as it is turbulent and thus its Reynolds number is high. Nonetheless, Figure 9 shows that we can still compute a vector field which seems to be accurate by visual inspection. Figure 10 compares the results of the control approach to the results of the Horn&Schunck approach. Please note that while Horn&Schunck seems to underestimate the curl, the control approach is able to recover the individual vortices more accurately.

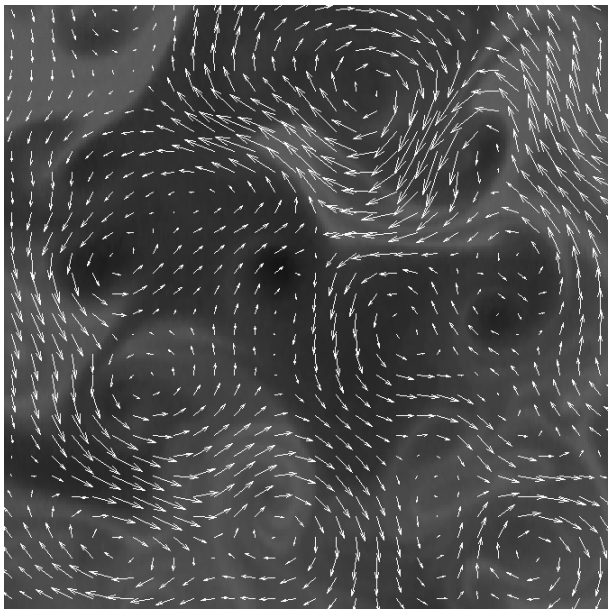

Fig. 9. Real image and its incompressible 2D flow field.

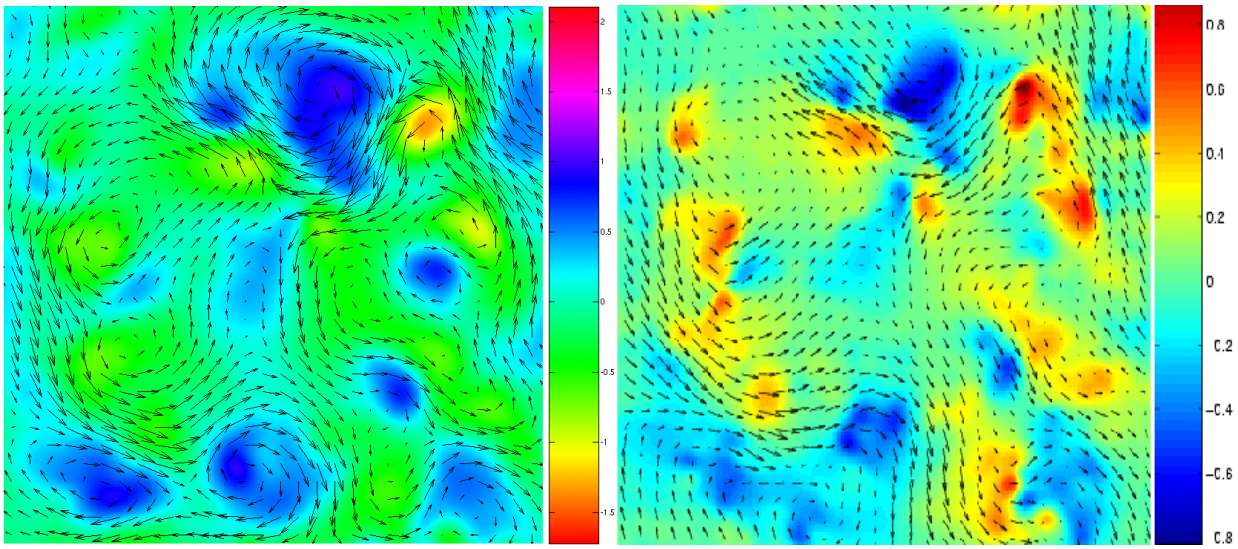

Fig. 10. Left: Resulting velocity field of control approach and its curl. Right: Resulting velocity field of Horn&Schunck approach and its curl.

5. Conclusions and Further Work

We presented a novel variational flow control approach for PIV that uses the Stokes equation as prior knowledge. Methods from flow control were used to solve the arising constrained optimization problem. The experimental evaluation showed that, as long as we confine ourselves to flows that are actually governed by the Stokes equation, the proposed algorithm is not only capable of reliably estimating the velocity fields between image pairs, but it can also extract the pressure distribution and forces acting on the fluid.
Our future work will concentrate on two main aspects: The assumption of a vanishing divergence in 2D is usually not valid in real-world PIV sequences, as the out-of-plane velocity component is usually not negligibly small. Therefore, we will focus three-dimensional flow analysis in the future, because only in three dimensions it makes sense to impose physical contraints on real measurements. A second topic for future work is the need for better physical priors for environments with high Reynolds-numbers environments. We will incorporate the convection term of the Navier-Stokes equations, leading us to the study of involved non-linear constrained optimization problems.

Acknowledgement

Support by the Deutsche Forschungsgemeinschaft (DFG, SCHN 457/6) within the priority programme Bildgebende Messverfahren in der Strömungsmechanik (SPP-1147) is gratefully acknowledged.

[1] D. Braess. *Finite elements. Theory, fast solver, and applications in solid mechanics*. Springer, 1997.
[2] F. Brezzi and M. Fortin. *Mixed and hybrid finite element methods*. Springer New York, Inc.,, USA, 1991.
[3] Th. Corpetti, D. Heitz, G.Arroyo, E. Memin, A. Santa-Cruz. Fluid experimental flow estimation based on an optical-flow scheme. *Exp.Fluids*, 40(1):80-97, 2005.
[4] M. Gunzburger. *Perspectives in Flow Control and Optimization*. Soc. for Ind. and Appl. Math., USA, 2002.
[5] W. Hackbusch. *Iterative Solution of Large Sparse Systems of Equations*, vol. 95 *Appl Math.Sciences* Springer, 1993.
[6] B. Horn and B. Schunck. Determining optical flow. *Artificial Intelligence*, 17:185–203, 1981.
[7] A. Kaga, K Yamaguchi, A Kondo, and Y. Inoue. Combination of piv data with cfd using cost function method. In *Proc. 8th Int. Symp. on Flow Visualization*, page 257, 1998.
[8] T. Kohlberger, E. Memin, and C. Schnörr. Variational dense motion estimation using the helmholtz decomposition. In L.D. Griffin and M. Lillholm, ed., *Scale Space Methods in Computer Vision*, vol. 2695 of *LNCS*, pp. 432–448, 2003.
[9] L. D. Landau and E. M. Lifschitz. *Hydrodynamik*. #6 Lehrbuch der theoretischen Physik. Harri Deutsch, 1952.
[10] J.L. Lions. *Optimal Control of Systems Governed by Partial Differential Equations*. Springer, 1971.
[11] Z. Michaewicz. *Genetic Algorithms + Data Structures = Evolution Programs*. Springer, 1994.
[12] H.H. Nagel and W. Enkelmann. An investigation of smoothness constraints for the estimation of displacement vector fields from image sequences. *IEEE Trans. Patt. Mach. Intell.*, 8(5):565–593, 1986.
[13] H. Nobach, N.T. Ouellette, E. Bodenschatz, and C. Tropea. Full-field correlation-based image processing for piv. In Proc. *6th Int. Symposium on Particle Image Velocimetry*, Pasadena, California, USA, September 21-23, 2005.
[14] H. Nobach, and C. Tropea. Improvements to piv image analysis by recognizing velocity gradients. *Exp. Fluids*, 39:614-622, 2005.
[15] K. Ogawara, T. Noborizato, and S. Iida. A moving least square piv algorithm coupled with navierstokes flow solver. In *Proc. 2nd Int. Workshop on PIV'97*, 1997.
[16] K. Okamoto, S. Nishio, and T. Kobayashi. Standard images for particle-image velocimetry. *Meas. Sci. Technol.*, 11:685–691, 2000.
[17] T. Okuno, S. Yasuhiko, and S. Nishio. Image measurement of flow field using physics-based dynamic model. *Meas. Sci. Technol.*, 11:667–676, 2000.
[18] P. Ruhnau, C. Guetter, and C. Schnörr. A variational approach for particle tracking velocimetry. *Meas. Sci. Technol.*, 16(7):1449–1458, 2005.
[19] P. Ruhnau, T. Kohlberger, H. Nobach, and C. Schnörr. Variational optical flow estimation for particle image velocimetry. *Exp. Fluids*, 38:21–32, 2005.
[20] C. Schnörr. Determining optical flow for irregular domains by minimizing quadratic functionals of a certain class. *International Journal of Computer Vision*, 6(1):25–38, April 1991.